


Article

Modeling and Performance Analysis of Municipal Solid Waste Treatment in Plasma Torch Reactor

Samira Elaissi *  and Norah A. M. Alsaif

Department of Physics, College of Science, Princess Nourah Bint Abdulrahman University, P.O. Box 84428, Riyadh 11671, Saudi Arabia

* Correspondence: saelaissi@pnu.edu.sa

Abstract: Thermal plasma has emerged as a technology with tremendous promise for municipal wastes that should be disposed of sustainably. A numerical simulation of a symmetric turbulent plasma jet from a thermal air plasma torch was developed using COMSOL Multiphysics®5.4 engineering simulation software. The velocities, temperature, arc root motion, and joule heating of the plasma jet were examined under the impact of the gas mass flow rate and current. Moreover, the electrical power required for the municipal solid waste (MSW) processing was estimated. The enthalpy and the effectiveness of the plasma torch were analyzed and discussed. Subsequently an investigation was conducted into the gasification characteristics of MSW using air and steam gases. The torch's power and efficiency could be enhanced with a higher mass flow rate and temperature. Three operating modes were identified from the current–arc flow combination. Among the plasma gas considered, the air gas plasma torch guarantees an acceptable thermal efficiency and a low anode erosion rate. Plasma gasification produces cleaner syngas with higher efficiency (84%) than the conventional process due to the elevated temperature used during the process that breaks down all the char, dioxins, and tars.

Keywords: thermal plasma torch; air; steam; turbulence; plasma jet; municipal solid waste (MSW); modeling



check for updates

Citation: Elaissi, S.; Alsaif, N.A.M. Modeling and Performance Analysis of Municipal Solid Waste Treatment in Plasma Torch Reactor. *Symmetry* **2023**, *15*, 692. <https://doi.org/10.3390/sym15030692>

Academic Editor: Alexander B. Kukushkin

Received: 4 February 2023

Revised: 22 February 2023

Accepted: 2 March 2023

Published: 10 March 2023



Copyright: © 2023 by the authors. Licensee MDPI, Basel, Switzerland. This article is an open access article distributed under the terms and conditions of the Creative Commons Attribution (CC BY) license (<https://creativecommons.org/licenses/by/4.0/>).

1. Introduction

Developing countries face a crucial problem due to the exponential increase in industrial development and population consumption, which are causing massive growth in solid municipal waste generation [1]. There is an increasing concern regarding the environmental pollution, health risks, and lack of sustainability of pathological, sharp, infectious, and chemical wastes [2–4]. The world health organization has classified municipal solid wastes (MSW) as hazardous wastes [5].

Autoclave and microwave systems are capable of disinfecting MSW. However, these technologies are not able to reduce the waste volume or to use the MSW as an energy source [6]. Waste recycling and energy recuperation can be improved significantly through pyrolysis, gasification, and incineration, which are regarded as thermal waste treatment mechanisms [7]. The gasification of MSW requires plasma as an energy source. Using plasma gasification melting (PGM) on municipal waste is highly effective, as the high temperatures that are involved organic waste conversion and pathogenic microorganism inactivation [8]. Several advantages make this technology ideally suited for MSW processing, such as its high thermal energy density, smaller reactors, easy control of the reaction temperature, and lower thermal losses. Its ability to operate independent of environmental gases, reduce pollution emissions, and treat a large amount of MSW are also notable benefits [9,10]. Electricity, which is an expensive source of energy, is the only disadvantage associated with this plasma process. However, electricity costs can be compensated by plasma's ability to process residues that cannot be treated using conventional methods [11].

This results in higher storage costs as well as an increase in the environmental impact. A common MSW sample contains 60–80% volatile species, which makes the mechanism of pyrolysis more intricated than that of biomass or coal [12].

A PGM reactor generally consists of an energy-supplying chamber in conjunction with one or multiple plasma torches providing energy for gasification reactions [13]. Direct-current (DC) electric discharge, including non-transferred or transferred discharge, radiofrequency (RF), and microwave discharge, enable a reactor to generate thermal plasma for waste treatment at atmospheric pressure [14]. DC plasma torches treat hazardous waste between two electrodes where high-temperature plasma extends, forming a plasma jet with high enthalpy [15]. Transferred electrodes incorporate the workpiece as a counter electrode, whereas the workpiece is integrated into a non-transferred-electrode torch by pushing plasma forward [16]. Radiofrequency induction plasma reactors prevent electrode erosion by generating a current through a coil surrounding the plasma chamber at a high frequency (2–27 MHz). However, RF torches are less flexible in terms of the plasma gas flow rate and torch power as well as heating efficiencies [17].

Several companies are developing technologies based on DC plasma torches for the treatment of industrial, agricultural, and hospital hazardous wastes [18]. In general, the product composition and economic process as well as energy efficiency are influenced by several operational factors, such as the suitable plasma torch, the temperature, the type of plasma gas, and the mass flow rate. Experiments, which are expensive and time-consuming, are often required to determine the optimal conditions for these parameters. Compared to experimental work, simulation models are required for exploring the waste materials behavior in a variety of reactors and to achieve ideal reactor conditions and define permissible limits while saving time and resources [19]. Several studies based on fluid dynamic modeling have been performed to clarify the involved phenomena. Li et al. [20] explained the vitrification mechanism of hazardous wastes using a thermodynamic equilibrium model of a 30 kW direct-current plasma torch. Tang et al. [21] have studied the plasma power effect, the feed rate, and the particle size using a nitrogen plasma reactor for polypropylene pyrolysis. Moreover, a numerical simulation was developed by Moutouris et al. [22] that described plasma gasification in detail. Through the use of different operation conditions, Zhang et al. [23] determined the melting parameters of municipal solid waste gasification. On the other hand, Favas et al. [24] investigated the performance of a biomass gasifier based on the main operating variable parameters. Janajreh et al. [25] used an Aspen Plus model to identify different types of feedstocks. They showed that coal and tire waste material can generate high gasification efficiency.

In this study, COMSOL Multiphysics[®]5.4 software conditions [26] were used to develop a computational fluid dynamic (CFD) simulation of a DC transferred plasma torch under a steady state. Hydrodynamic flow simulations were used to examine the treatment of hazardous municipal solid wastes using thermal plasma. The influences of operating conditions, such as the mass flow rate and plasma current, were analyzed in terms of velocities, temperature, arc root motion, and joule heating. Moreover, the estimation of the electrical power required in the MSW was determined, as well as the efficiency and the enthalpy of the plasma torch were analyzed and discussed.

The simulation model was used to determine the energy requirement and energy balances for an air plasma arc gasification reactor. To evaluate the plasma gasification cycle's suitability for recovering energy from wastes, operating conditions were optimized and plasma gasification performance was analyzed. Numerical simulations are useful for improving the control and composition of produced syngas to obtain a higher heating temperature and a low harmful emission concentration. These research results can be extended to other waste materials, such as medical wastes and nuclear wastes.

2. Technology of Waste Treatment Setup

Hazardous waste compounds can be thermally decomposed into benign and simpler materials using plasma reactors. Plasma reactors reduce wastes in a stable and non-

leachable glassy slag phase (in the range of 1400–1600 °C melting points) [27]. As a result of the vitrification process, substances are treated, offering products that are safely re-used, such as scrap metals [28]. In addition, using gasification or pyrolysis, these dangerous substances can be transformed into a synthetic gas (syngas) employed as a fossil fuel [29]. Consequently, there are three categories of waste treatment with plasma technology [30]: (a) plasma pyrolysis, which breaks down chemical compounds; (b) plasma gasification melting, which converts organic compounds into combustible gases to produce electric power; and (c) plasma vitrification, which converts wastes into vitrified ceramics by adding a suitable flux material. Figure 1 depicts a schematic diagram of municipal waste treatment using thermal plasma.

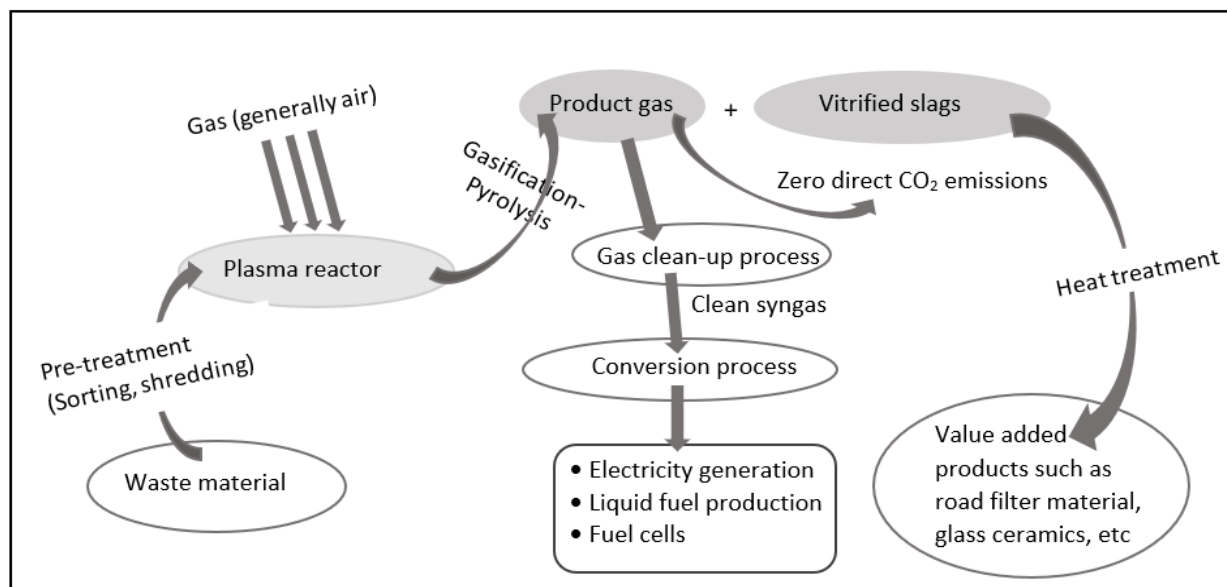


Figure 1. Schematic diagram of municipal solid waste treatment using thermal plasma.

The assumptions used in this model are the following [31]: (i) Solid wastes flow from the top to the bottom, whereas gases flow is from the bottom to the top. Reflux is not allowed during each phase. (ii) The components of ash-free fuel are C, H, and O. This model includes the gas-phase H_2 , H_2O , CO , CO_2 , O_2 , N_2 , CH_4 , C_2H_4 , and tars. (iii) The heat loss of each section is calculated from the measured temperature layout of the gasifier wall surface and the gasifier structure.

3. Plasma Reactor for MSW Gasification

Foundries use plasma gasification melting furnaces to remelt steel and scrap iron [32]. High temperatures and corrosive conditions are withstood by re-covering the furnace's interior with suitable refractory materials. Solid wastes are injected from the top (see Figure 2a). It is recommended to place the plasma torch at the bottom or at the top of the reactor to melt inorganic materials derived from non-living sources in solid wastes. Figure 2b presents an experimental setup of a plasma torch [33].

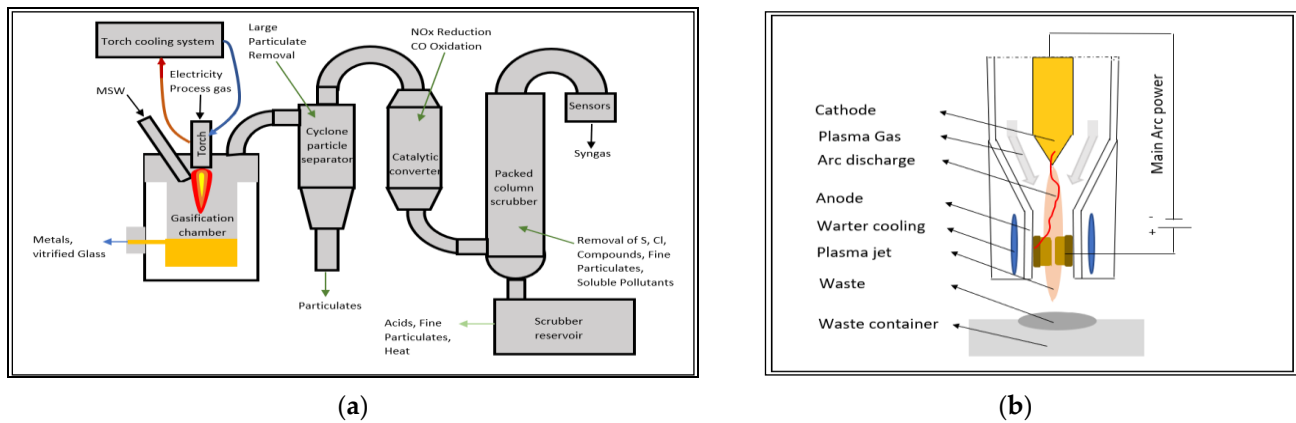


Figure 2. Diagram of plasma gasification melting process (a) and symmetrical plasma torch (b) used for municipal waste treatment.

During the plasma torch process, the system reaches high temperatures ($T > 5000\text{ }^{\circ}\text{C}$) with a maximum power between 75 kW and 10,000 kW. Table 1 lists the operational parameters of the arc plasma torch [24].

Table 1. Arc plasma torch's operational parameters of arc plasma torch.

Parameters	Values
Power	75–10,000 kW
Voltage	150–10,000 V
Current	500–1000 A
Plasma gas	Air
Air flow rate	4–10 g/s
Temperature of exit gas in plasma jet	5000–100,000 K
Pressure	1 atm

4. Mathematical Model

4.1. Assumption

The two-dimensional axisymmetric numerical model is used for an air arc discharge using the following assumptions: (i) plasma flow can be considered a continuous fluid in a local thermodynamic equilibrium and semi-compressible ($Ma < 0.3$); (ii) the gas has thin optical property; (iii) the arc flow is steady and turbulent; (iv) the swirl component is included; (v) the viscous dissipation is ignored; and (vi) temperature affects thermodynamic and transport properties [34].

4.2. Model Equations

The fluid dynamics model is described using Navier Stokes and Maxwell electromagnetic equations written in a cylindrical system [35]:

$$\nabla \cdot (\rho \mathbf{u}) = 0 \quad (1)$$

where ρ and \mathbf{u} represent the mass density and the velocity vector, respectively.

$$\nabla \cdot (\rho \mathbf{u} \mathbf{u}) = -\nabla p + \nabla \cdot \left\{ \Gamma_{\mu} \left[2\mathbf{S} - \frac{2}{3}(\nabla \cdot \mathbf{u})\mathbf{I} \right] \right\} + \mathbf{F}_L + \rho \mathbf{g} \quad (2)$$

where \mathbf{g} , p , and \mathbf{I} represent the gravity vector, the pressure, and the unit vector, respectively. \mathbf{F}_L is the body force, including the Lorentz force. \mathbf{S} is the strain-rate tensor velocity, written as

$$\mathbf{S} = \frac{1}{2} \left[(\nabla \mathbf{u}) + (\nabla \mathbf{u})^{\text{tr}} \right] \quad (3)$$

The superscript (^{tr}) denotes that the matrix transposes the operation.

$$\nabla \cdot (\rho h \mathbf{u}) - \nabla \cdot (\Gamma_\kappa \nabla h) = Q_p - Q_{\text{rad}} \quad (4)$$

in which Γ_κ , h , Q_p , and Q_{rad} are the thermal conductivity, the gas enthalpy, the production heat, and the radiation losses, respectively.

Considering thermal plasmas as electronically neutral, the resulting force is the Lorentz force:

$$\mathbf{F}_L = \mathbf{J} \times \mathbf{B} \quad (5)$$

The production heat is calculated as

$$Q_p = \mathbf{J}(\mathbf{E} + \mathbf{u} \times \mathbf{B}) \quad (6)$$

Based on the following equation, the radiative flux is approximated [36]:

$$Q_{\text{rad}} = 4\pi\epsilon_r \quad (7)$$

where \mathbf{J} corresponds to the density vector of the electric current, and \mathbf{B} and \mathbf{E} denote the magnetic field and the electric field, respectively. The effective net emission coefficient is denoted by ϵ_r , expressed as a function of the temperature.

In electric arc modeling, Ohm's law is used:

$$\mathbf{J} = \sigma (\mathbf{E} + \mathbf{u} \times \mathbf{B}) \quad (8)$$

where the electric conductivity is represented by σ . The electrical field and potential (ϕ) can be related using the following equation:

$$\mathbf{E} = -\nabla\phi \quad (9)$$

The relationship between the magnetic field (\mathbf{B}) and the magnetic vector potential (\mathbf{A}) is given by:

$$\mathbf{B} = \nabla \times \mathbf{A} \quad (10)$$

The equation of Maxwell–Ampere is:

$$\Delta \times \mathbf{B} = \mu_0 \mathbf{J} \quad (11)$$

where μ_0 is the vacuum permeability.

Considering the high reactivity, large property variation, and electromagnetic effect of thermal plasma flow, turbulence models are significantly approved [37]. The ($\mathbf{K} - \epsilon$) turbulence model is used with the below equations for the turbulent kinetic energy (\mathbf{K}) to describe the turbulent plasma jet:

$$\nabla \cdot (\rho \mathbf{u} \mathbf{K}) - \nabla \cdot (\Gamma_K \nabla \mathbf{K}) = G - \rho \epsilon \quad (12)$$

and the turbulent dissipation rate (ϵ):

$$\nabla \cdot (\rho \mathbf{u} \epsilon) - \nabla \cdot (\Gamma_\epsilon \nabla \epsilon) = \frac{\epsilon}{\mathbf{K}} (C_1 G - C_2 \rho \epsilon) \quad (13)$$

In these equations, the production term (G) is given by

$$G = \mu_t \left[\nabla \mathbf{u} : (2\mathbf{S}) - \frac{2}{3} (\nabla \mathbf{u})^2 \right] - \frac{2}{3} \rho \mathbf{K} \nabla \cdot \mathbf{u} \quad (14)$$

Γ_κ , Γ_μ , Γ_ϵ , and Γ_K are defined, respectively, as

$$\Gamma_\kappa = \kappa + \frac{\mu_t C_p}{Pr_t} \quad (15)$$

$$\Gamma_{\mu} = \mu + \mu_t \quad (16)$$

$$\Gamma_{\varepsilon} = \mu + \frac{\mu_t}{\sigma_{\varepsilon}} \quad (17)$$

$$\Gamma_K = \mu + \frac{\mu_t}{\sigma_K} \quad (18)$$

C_p , κ and μ represent, respectively, the specific heat at a constant pressure, the thermal conductivity, and the viscosity coefficient. The turbulent kinematic viscosity (μ_t) is given by

$$\mu_t = \rho C_{\mu} \frac{K^2}{\varepsilon} \quad (19)$$

and the turbulent constants are considered at the following values [38]:

$$C_1 = 1.44, C_{\mu} = 0.09, C_2 = 1.92, \sigma_{\varepsilon} = 1.3, \sigma_K = 1, \text{ and } Pr_t = 0.9.$$

The following boundary conditions are applied in this physical model:

A radial velocity ($v = 0$) is set at the plasma torch's inlet, while the axial velocity is defined as

$$u = \dot{m} / \rho A_{\text{inlet}} \quad (20)$$

where \dot{m} , A_{inlet} , and ρ are, the mass flow rate, the torch inlet area, and the density of gas respectively.

By introducing air cyclone into the torch's inlet, an induced flow is produced with an azimuthal velocity written as

$$w = \frac{k_1}{r} \quad (21)$$

The intensity of the free vortex is determined by the distinct values of k_1 [39].

The injected air temperature is 300 K in the heat transfer in the fluid. At the cathode-tip, a temperature of 3500 K is applied, while a grounded potential is adopted at the external anode surface. Q_{ex} represents the transfer of the convective heat from the anode's outer side, which is externally cooled by the cooling water:

$$Q_{\text{ex}} = h_{\text{conv}} (T_{\text{wall}} - T_{\text{water}}) \quad (22)$$

where h_{conv} represents the coefficient of convective heat transfer ($h_{\text{conv}} = 10^4 \text{ W/m}^2 \text{ K}$), and T_{wall} and T_{water} represent the wall temperature and the cooling water temperature (500 K), respectively [40].

The following equation represents the density profile of the radial current applied at the cathode tip:

$$J(r) = J_{\text{max}} \left[1 - \left(\frac{r}{R_{\text{arc}}} \right)^n \right] \quad (23)$$

The parameters r and n specify the radial position from the axis of the torch and the form of the distribution of current density. J_{max} and the arc core radius (R_{arc}) represent respectively the maximal current density around the torch axis, and the radial distance between the cathode tip and the end of the arc.

At the outlet, an atmospheric pressure is imposed. The other boundaries of the torch are electrically insulated. All external boundaries are magnetically insulated, and the potential vector (A) is defined with a gauge fixed at 1 A/m [41].

A temperature of 300 K and an atmospheric pressure are initially imposed on the whole domain. Table 2 shows the boundary conditions.

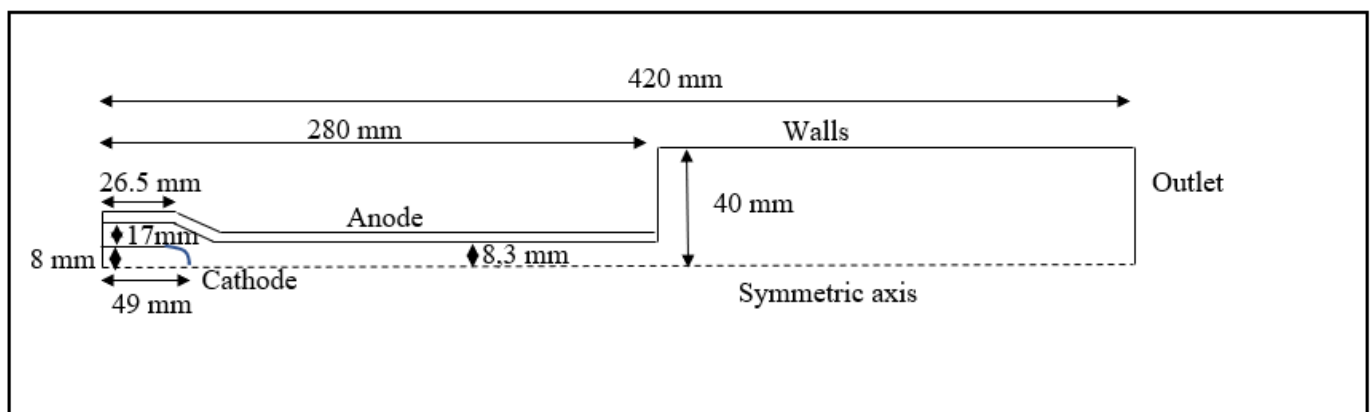
Table 2. Boundary conditions.

	Inlet	Outlet	Walls	Anode	Cathode Tip	Cathode
u (m/s)	$\dot{m}/\rho A_{\text{inlet}}$	$\partial_n u = 0$	0	0	0	0
v (m/s)	0	$\partial_n v = 0$	0	0	0	0
w (m/s)	6.1 to 19.1	$\partial_n w = 0$	0	0	0	0
T (K)	300	$\partial_n T = 0$	$\partial_n T = 0$	$Q_{\text{ex}} = h_{\text{conv}}(T_{\text{wall}} - T_{\text{water}})$	3500	$\partial_n T = 0$
ϕ (V)	$\partial_n \phi = 0$	$\partial_n \phi = 0$	$\partial_n \phi = 0$	0	$-\sigma \partial_n \phi = J(r)$	$\partial_n \phi = 0$
P (Pa)	$\partial_n P = 0$	1.013×10^5	$\partial_n P = 0$	$\partial_n P = 0$	$\partial_n P = 0$	$\partial_n P = 0$
A_r (T·m)	$\partial_n A_r = 0$	0	$\partial_n A_r = 0$	$\partial_n A_r = 0$	$\partial_n A_r = 0$	$\partial_n A_r = 0$
A_z (T·m)	$\partial_n A_z = 0$	0	$\partial_n A_z = 0$	$\partial_n A_z = 0$	$\partial_n A_z = 0$	$\partial_n A_z = 0$
A_ϕ (T·m)	$\partial_n A_\phi = 0$	0	$\partial_n A_\phi = 0$	$\partial_n A_\phi = 0$	$\partial_n A_\phi = 0$	$\partial_n A_\phi = 0$
u (m/s)	$\dot{m}/\rho A_{\text{inlet}}$	$\partial_n u = 0$	0	0	0	0
v (m/s)	0	$\partial_n v = 0$	0	0	0	0

Air properties including the specific heat, thermal conductivity, density, electrical conductivity, enthalpy, and dynamic viscosity depend on the temperature variation and were taken from ref. [42]. The net emission coefficient calculated for the source radiation was taken from ref. [43].

4.3. Simulation Domain and Parameters

The simulation domain of the discharge region and the plasma jet zone is illustrated in Figure 3. The gas inlet radius and the cathode were respectively 17 mm and 8 mm. The cathode tip had a 2 mm radius, and the radial distance between the torch axis and the anode was 8.3 mm. The DC arc plasma model was constructed based on the theories of the equilibrium plasma discharge interface, electromagnetism, heat transfer and fluid mechanics. A finite element Galerkin method was utilized to solve the coupled partial differential equations using COMSOL Multiphysics[®]5.4 software [44] to conduct two-dimensional axisymmetric modeling. The MUMPS direct solver is used to numerically integrate model equations, and the solved number of degrees of freedom is equal to 1.7×10^6 .

**Figure 3.** Symmetrical diagram of plasma torch.

For accurate results, a grid independency study was conducted to determine the number of meshes and the mesh quality. Simulations of the flow domain were repeated for three different computational meshes (coarse: 988,078; fine: 1,527,606; and finest: 2,147,061) to select the suitable mesh for the optimization study.

Figure 4a shows the temperature profiles along the axial axis of three types of grid sizes (at $r = 0$ mm and x varies between 0 and 80 mm) for a plasma gas flow rate of 23.6 LPM and 10.8 kW of input power. The use of a coarse grid led to a significant difference in optimizing the mesh along the temperature distribution, while, the fine grid agreed well with the finest one.

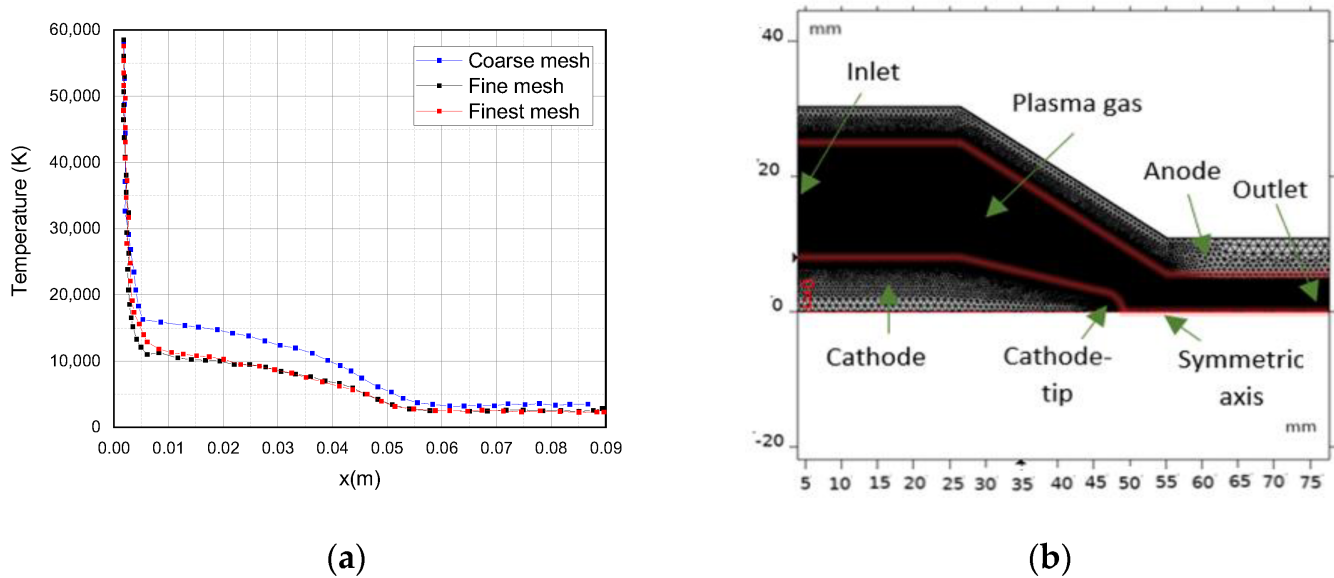


Figure 4. (a) Axial temperature profiles using different meshes. (b) Plasma torch computational grid.

To achieve reasonable results while taking into consideration computational cost, the fine mesh grid is used in this study. Due to the sharp change in the gas flow direction at the electrode tip, denser meshes were generated with the smallest cells in this region, as shown in Figure 4b. There was a refinement in the discretization near the inner walls. The computational domain of the torch was meshed with approximately 1.8×10^6 triangle elements.

5. Results

To demonstrate the model's accuracy, a comparison of the simulation results and experimental measurements of axial velocity and temperature profiles is performed. Moreover, a study was conducted to determine the impacts of the current and the mass flow rate on the plasma velocity and temperature distributions. The dissipated power, the enthalpy, and the efficiency are discussed to clarify their effects on the mechanical performance of the torch for MSW treatment.

5.1. Comparison with Experimental Data

According to Figure 5, the axial velocity and the plasma temperature along the symmetry axis were compared theoretically and experimentally [45]. A laser doppler anemometry (LDA) system was used to measure the mean velocity and intensity of the turbulence, where $1 \mu\text{m}$ Alumina particles were injected directly into the torch anode to seed the plasma flow, whereas temperature measurements were carried out using emission spectroscopy and enthalpy probe techniques [46]. An acceptable agreement was obtained along 30 mm of the symmetry axis.

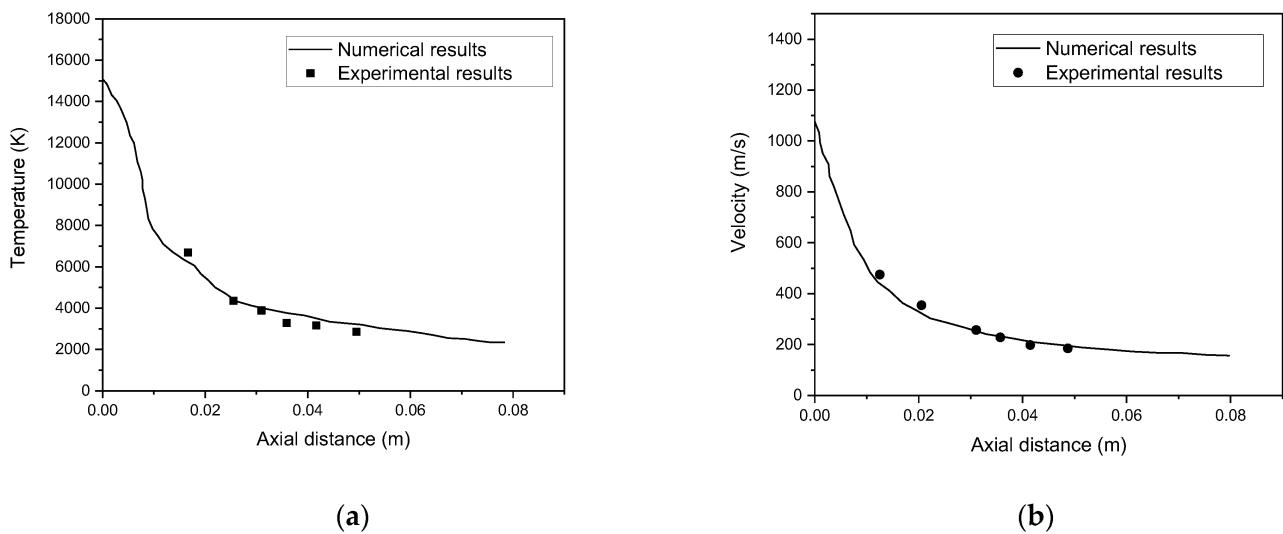


Figure 5. Comparison with experimental data of (a) axial temperature and (b) axial velocity.

5.2. Velocity and Temperature Evolution in the Plasma Torch

Figure 6 represents the temperature and velocity distributions for an air flow rate of 5 g/s and a 500 A electrical current. The temperature of plasma reaches its extreme value around the cathode tip. Whereas, leaving the cathode, the irradiation and convective thermal losses became more pronounced [47], and the plasma jet's temperature decreased in the axial and radial directions. Simultaneously, the velocity of the jet augmented, and its maximum magnitude is reached at the outlet center. This was caused by gas expansion from Joule heating [48]. A DC arc discharge produced a high temperature and energy density between two electrodes in an arc plasma torch. When sufficient gas flow rate was present, the plasma spread beyond one electrode, creating a plasma jet [49]. The plume temperature could exceed 1×10^4 °C at the core of the plasma and could reach as high as 5000 °C in the marginal zone.

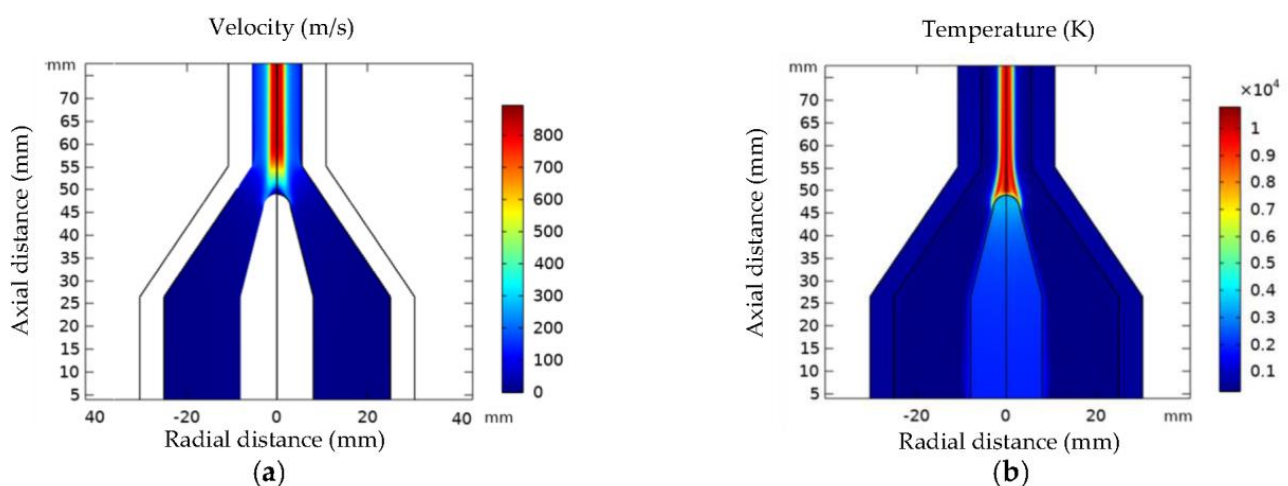


Figure 6. Velocity (a) and temperature (b) distributions of air in a non-transferred plasma torch. $I = 500$ A and $\dot{m} = 5$ g/s.

5.3. Influence of Plasma Current

Figure 7 illustrates the mean voltage variation versus the electric current varying between 500–620 A and with a 5 g/s air flow rate. This figure illustrates that an increase in the plasma current led to a higher voltage and increased the vaporization of waste [50].

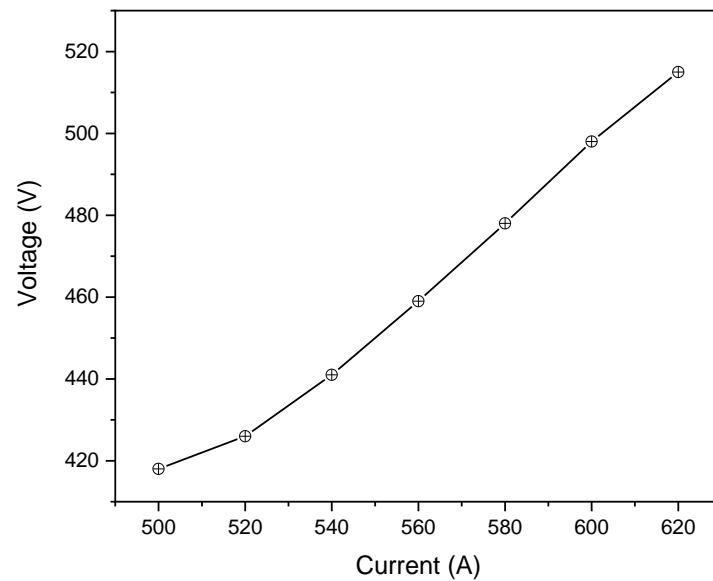


Figure 7. Mean voltage versus discharge current ($\dot{m} = 5$ g/s).

Figure 8 displays the radial distributions of the velocity and temperature at the torch exit of the plasma jet for various currents ($I = 500, 600,$ and 800 A). According to Figure 8a, the more the current increased, the more the arc core temperature rose and its temperature profile became wider. As a result of this higher temperature, an elevated arc root velocity was obtained (see Figure 8b).

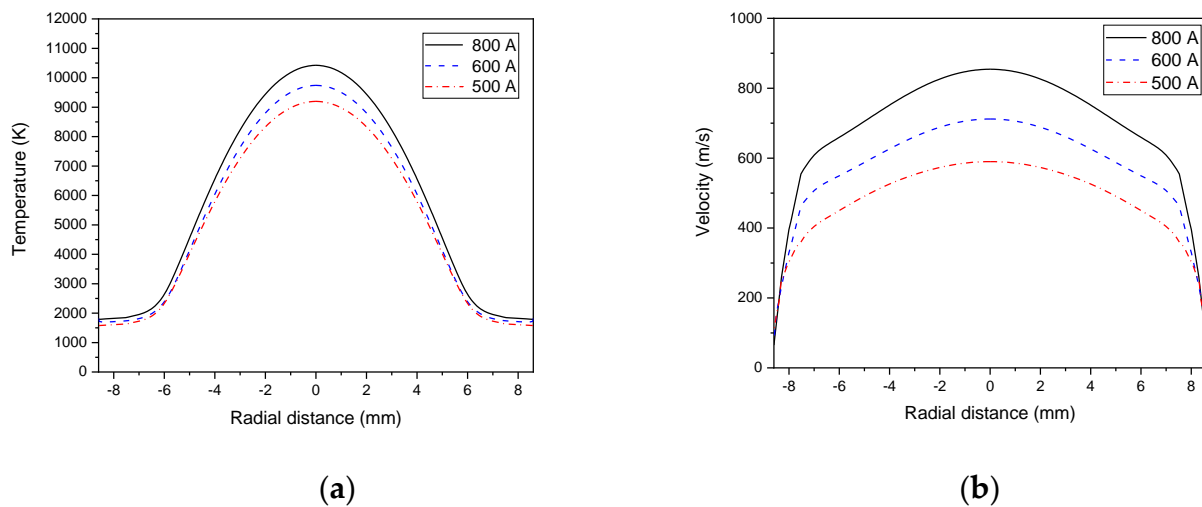


Figure 8. Radial distributions of plasma jet temperature (a) and velocity (b) profiles at the torch exit for various currents ($I = 500, 600,$ and 800 A) and $\dot{m} = 5$ g/s.

5.4. Influence of Air Mass Flow Rate

The air mass flow rate effect was examined over a range of (4–10 g/s) for a 500 A current. As displayed in Figure 9, the voltage rised at a higher air mass flow rate. Furthermore, this led to increases in the convection heat transfer and non-equilibrium effects, and arc cooling occurred more rapidly. Consequently, larger instabilities were observed to be caused by a greater voltage drop.

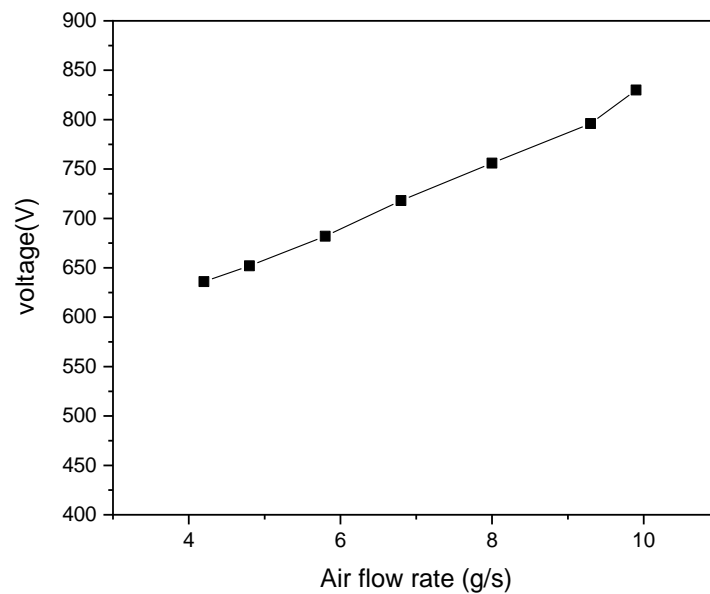


Figure 9. Voltage variation with air mass flow rate ($I = 500$ A).

Figure 10 illustrates the maximum temperature of the plasma jet as a function of the air mass flow rate at various cathode-tip temperatures. With increasing mass flow rates of gas, the maximum temperature of plasma jet decreased. As a result, the radial and axial thermal gradients were reduced. However, a torch characterized by a lower mass flow rate will not necessarily have a higher nozzle exit temperature [51].

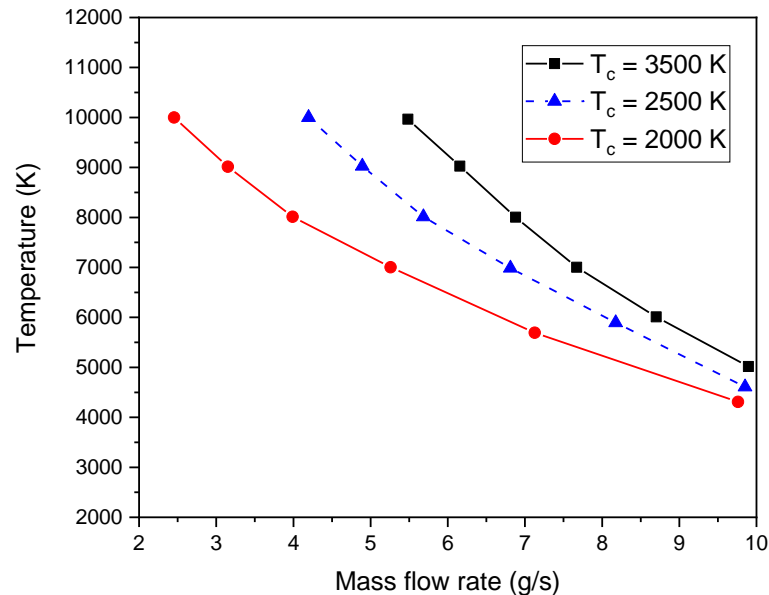


Figure 10. Plasma temperature variation with air mass flow rate.

Figure 11 displays the velocity profiles and the radial temperatures at the torch exit for different mass flow rates. Despite this decrease in the maximum temperature at a higher mass flow rate (seen in Figure 10), the temperature at the nozzle exit was still elevated. Indeed, Figure 11a shows that the maximum temperatures reached in the center of the arc core with the three mass flow rates were very close. Furthermore, lower mass flow rates resulted in wider temperature profiles. In fact, since the arc core temperature was mainly determined by the current, the outline of the arc core was cooled by mass flow.

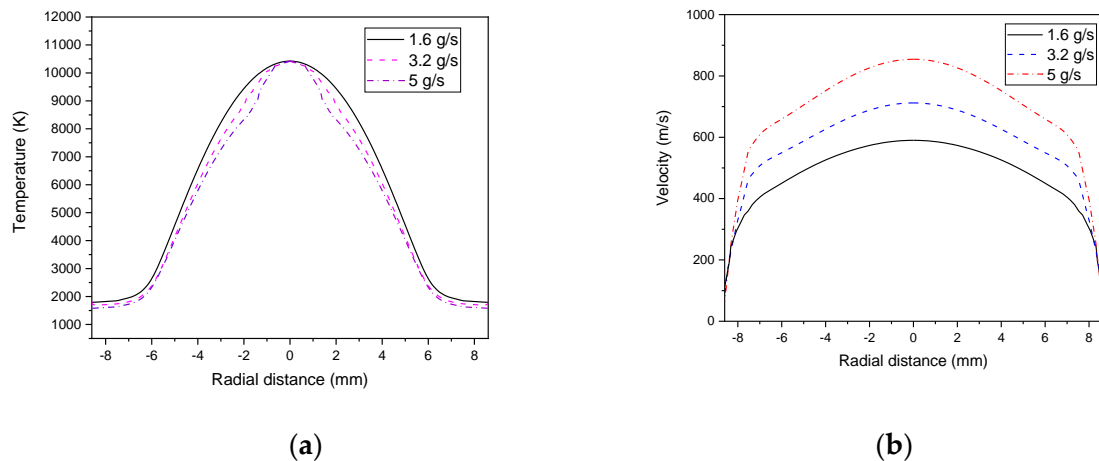


Figure 11. Radial distributions of plasma jet temperature (a) and velocity (b) profiles at the torch exit for various air mass flow rates ($I = 500$ A).

As shown in Figure 11b, the velocity achieved maximum values of 495 m/s with 1.6 g/s and 806 m/s with 5 g/s. In addition, turbulence caused distortion of the velocity profile at higher air flow rates.

5.5. Deposited Power

The power supply plays a crucial role in the disposal of an MSW system since it determines the torch processing capacity. Based on the torch energies balance, the produced vitrified mass is determined by [26]:

$$M \text{ (kg)} = 0.35 \times P \text{ (kWh)} \quad (24)$$

where P represents the power in kilowatt hours (kWh)

Further, the power supply is necessary for sustaining the plasma in the reactor and supplying the process with an operational control system [52].

Under different discharge currents, the plasma torch power variation with the rate of air mass flow is illustrated in Figure 12. The torch power consumption increased as the rate of air mass flow increased from 1 to 6 g/s.

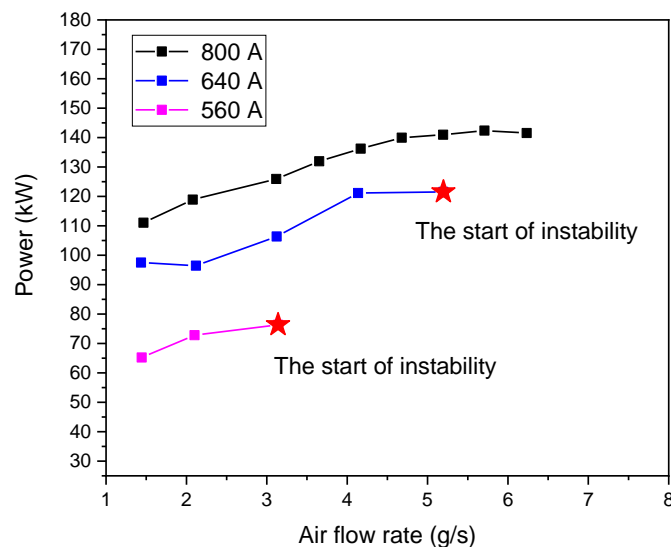


Figure 12. Power variation as function of mass flow rates of air at various current values ($I = 560, 640,$ and 800 A).

With an increasing current, from 560 to 800 A, the deposit power increased. Indeed, the average arc temperature rose when increased current, and generated higher electrical conductivity, which dissipated more power in this region.

Moreover, as the current increased, the magnitude of the instabilities decreased, and a stable flow of plasma jet was generated. However, a high current can adversely affect the anode and cathode's longevity. In contrast, plasma jets produced by small currents are short and narrow, with low energy density to gasify solid waste.

A plasma torch can operate in three distinct modes based on current and arc flow analysis: the restrike mode, the takeover mode, and the steady mode [53]. There is a correlation between the operation modes and the cold gas boundary layer thickness within the arc and the anode nozzle wall. Restrike mode is recommended with intensive boundary layer, whereas steady mode is desired with a fine boundary layer. (i) At 560 A, highly transient dynamic phenomena occurred, and the arc column was highly distorted because of strong fluctuation plasma flow. A thicker boundary layer was established leading to a restrike mode operation. (ii) Increasing the arc current (640 A) decreased the boundary layer thickness. The anode showed a thinner boundary layer and reduced motion of the arc attachment, leading to operation in takeover mode. (iii) At a higher current (800 A), the anode attachment movement was attenuated, and a thin boundary layer favored operation in the steady mode.

To illustrate the flow instabilities, Figure 13 displays the plasma jet velocity distribution. Symmetric vortexes were progressively created on either side of the plasma jet core, causing the mixing layer's mean velocity to increase. These results are in accordance with those given by Trelles et al. [54]. The results indicate that the entrainment of the cold gas around the plasma jet generated instabilities and turbulence flow. The axial jet velocity dropped rapidly due to the slow dissipation of the cold engulfed gas bubbles through molecular diffusion when air molecular gases were entrained.

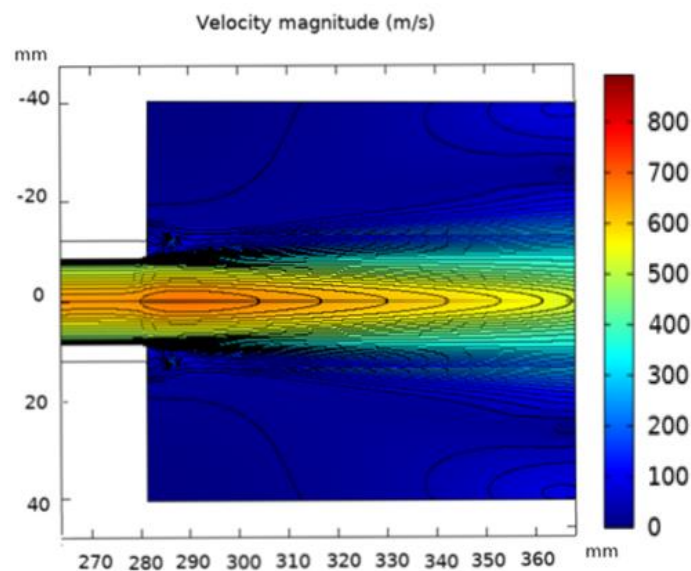


Figure 13. Velocity distribution, illustrating the instabilities ($\dot{m} = 5$ g/s and $I = 500$ A).

According to Figure 14, torch power consumption varied with the plasma temperature for various cathode tip-temperatures. As the cathode-tip temperature increased from 2000 to 3500 °C, the torch power rose by 20% for plasma temperatures of 5000 K and by 40% for plasma temperatures of 10,000 K. Therefore, at a constant plasma temperature, a high power was achieved by increasing the torch's energy supply and its airflow rate according to the reactor energy balance (as seen in Figure 11).

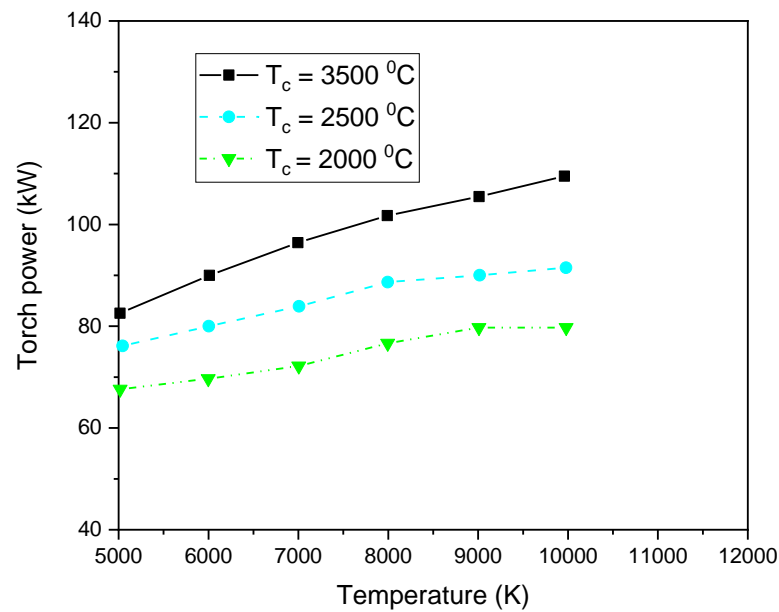


Figure 14. Torch power consumption with plasma temperature for various cathode-tip temperatures.

Figure 14 illustrates the influence of plasma power on gasification and the average pyrolysis temperature. The plasma temperature increased linearly with the plasma power. Indeed, the plasma power enhanced the feeding air temperature and raised the amount of heat available for pyrolysis and gasification [55]. Hence, the combustible gas increased with the plasma power by increasing the pyrolysis temperature. Thus, the plasma power has the potential to increase syngas yield and quality, while increasing the plasma power has limited beneficial effects.

Figure 15 illustrates the torch power change according to the length of the arc core radius with a 500 A current and a 5 g/s gas flow rate. Increasing the axial distance between the anode arc spot and the cathode tip augmented the torch power, while increasing the arc core radius diminished it.

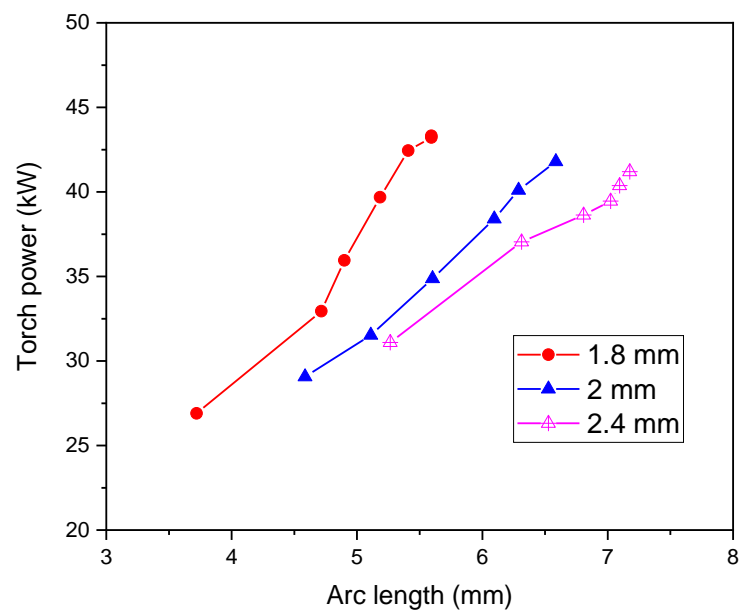


Figure 15. Torch power as function of axial distance for various arc core radii (1.8–2.4 mm).

5.6. Enthalpy

The purpose of plasma torches is to transform electrical energy into thermal energy at stable an electrical discharge. With high-enthalpy plasma, the gas interacts widely with the electric arc, resulting in a higher conversion efficiency that can exceed 90%, depending on which plasma torch and working gas are used [56].

The average value of enthalpy is one of the main parameters when treating waste using thermal plasma. It is expressed as the energy balance of the plasma torch [57]:

$$\dot{m} h_{\text{ave}} = IV - Q_{\text{loss}} \quad (25)$$

where V represents the arc voltage and I is the arc current. Q_{loss} is the dissipated power by water used to cool the electrode, given by

$$Q_{\text{loss}} = \dot{m} \times C_p \times (T_2 - T_1) \quad (26)$$

where \dot{m} and C_p represent the mass flow rate, and the specific heat capacity respectively, T_1 is the inlet temperature, and T_2 is the cooling water outlet temperature.

Argon, air, and steam represent the plasma gases considered in this study. In fact, argon is the most used common technical plasma gas. Air is abundant, and due its low specific heat, leading to a low energy input, it can achieve the required high temperature [58]. When compared with argon, air has the advantage that the electrodes tend not to oxidize [59].

A plasma torch can be supplied with water as a liquid or as generated steam. In addition to its interesting physical property and its obvious economic advantages, water has many advantages as a plasma gas compared to noble gases [60].

For different types of plasma gas, Figure 16 represents the plasma enthalpy as a plasma temperature function. While a plasma arc is likely to be formed with argon gas, the obtained energy density is low and the plasma jet is too short, leading to a less effective gasification. When compared with air, steam provides more hydrogen and more oxygen to the process. However, due to the elevated specific heat and absorbed latent heat of evaporation, steam requires more energy to be input, which makes it expensive.

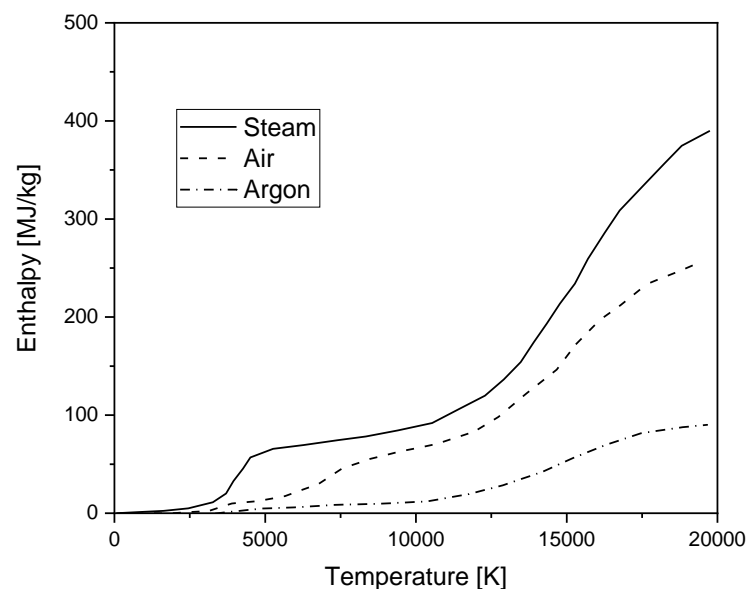


Figure 16. Plasma enthalpy as a function of the plasma flame temperature for different working gases at the same mass flow rate and $\dot{m} = 5 \text{ g/s}$.

5.7. Efficiency

In a gasification process, gas efficiency is frequently used as a standard criterion that expresses the energy efficiency. The electro-thermal efficiency is measured using the following equation [61]:

$$\eta = \frac{I \cdot V - Q_{\text{loss}}}{I \cdot V} \times 100 \quad (27)$$

Figure 17 displays the plasma efficiency variation according to the plasma temperature. There was a strong correlation between plant efficiency and the plasma temperature, which was highly influenced by the consumption of torch power. The efficiency of the plant increased by 8% when the temperature of the plasma was raised from 5000 to 10,000 °C.

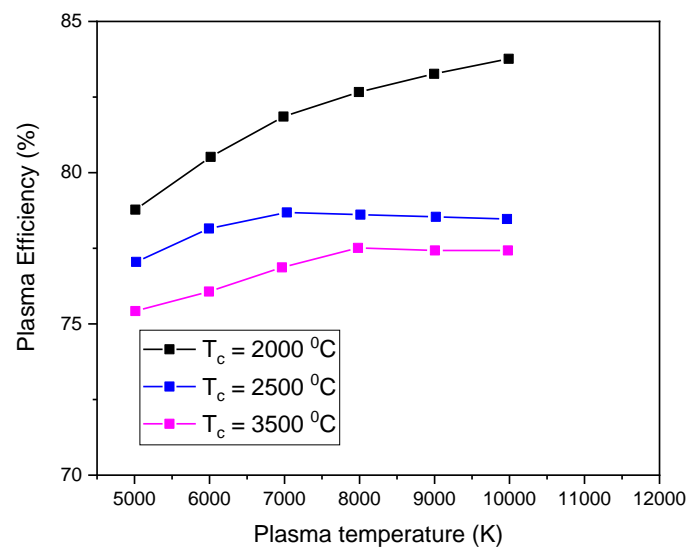


Figure 17. Plasma efficiency according to the plasma temperature.

Figure 18 displays the plasma efficiency variation according to the gas mass flow rate. The torch's power and efficiency were enhanced by increasing the gas mass flow rate. However, as the current increased, the efficiency decreased. Increasing the current caused the arc channel near the anode spot to be stronger. Therefore, a higher heat loss through this channel was observed [62].

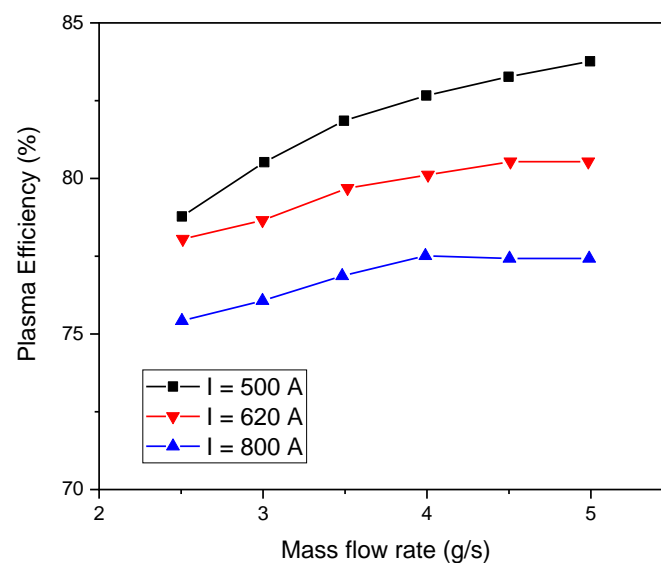


Figure 18. Plasma efficiency variation according to the mass flow rate of gas.

According to the first and second laws of thermodynamics [63], plasma gasification melting exhibits low efficiency at a lower power. This can be explained by three reasons: firstly, the design of the gasification reactor; secondly, the plasma torch's stability; and thirdly, the system's heat loss. Indeed, with a small-scale system gasification, residual carbon is produced due to the narrow space between the feedstock and the jet. Moreover, the power, which is important to gasification, is affected by the plasma torch's stability as well as the system's heat loss, where the dissipation and transformation of heat are influenced [64].

6. Conclusions

The purpose of this research paper is to investigate the thermal plasma torch mechanism applied in municipal solid waste treatment. To improve the efficiency of the plasma torch with respect to the conversion rate and power consumption, two-dimensional CFD modeling of the symmetric thermal plasma reactor was conducted. The plasma jet distribution of velocity and temperature were discussed. Several setups under different conditions were tested for the thermal destruction of MSW using DC plasma torches. The resulting analysis showed that a plasma torch can be operated in an optimal mode to maintain a stable flow with a highly efficient heating process.

The arc voltage increased in the DC plasma torch at a higher airflow rate, resulting in increases in plasma power and the average outlet temperature, allowing for full solid waste decomposition.

On the other hand, increasing the standard flow rate of the carrier gas reduced the max temperature of the anode plasma torch, which accelerated the plasma energy flow, improved plasma cooling on the arc boundaries, and enhanced protection of the anode. This increase in the gas flow rate was not unlimited because it reduced carrier gas ionization, and the thermal equilibrium state at the center of the arc is broken.

As the terminal current increased, the plasma torch maximum temperature rose, resulting in higher conductivity and a decrease in the arc voltage, while the arc power was simultaneously augmented because the average temperature rose both at the anode's inner wall and at the outlet of the plasma torch. Thus, waste treatment efficiency can be improved. However, this will also increase the anode loss rate by enhancing the anode wall temperature and shorten the anode's lifetime. Three operating modes can be identified from the current–arc flow combination, and they are strongly influenced by the cold gas boundary thickness between the arc and the anode nozzle wall. A thin boundary layer at a higher current favors a steady mode, while thick layers favor flow instabilities. A plasma gasification plant generates enthalpy of 250 MJ/kg and produces electric power with higher efficiency (84%) than conventional technologies based on waste incineration (20%) with fewer harmful pollutants. The air gas plasma torch presents the optimal torch operation among all the plasma gases considered because it ensures a low rate of anode erosion and an acceptable thermal efficiency. Plasma gasification produces cleaner syngas than the conventional process because of the high temperature that is used that breaks down all the char, dioxins, and tars.

Author Contributions: Conceptualization, methodology, software, validation, formal analysis, investigation, resources, data curation, writing—original draft preparation, writing—review and editing, visualization, and project administration, S.E. and N.A.M.A. All authors have read and agreed to the published version of the manuscript.

Funding: The authors extend their appreciation to the Deputyship for Research & Innovation, Ministry of Education in Saudi Arabia for funding this research work through the project number RI-44-0266.

Institutional Review Board Statement: Not applicable.

Informed Consent Statement: Not applicable.

Data Availability Statement: The data are contained within the article.

Acknowledgments: The authors would like to express their gratitude to the Deputyship for Research & Innovation, Ministry of Education in Saudi Arabia for funding this research work through the project number RI-44-0266.

Conflicts of Interest: The authors declare no conflict of interest.

References

1. Khan, S.; Anjum, R.; Raza, S.T.; Bazai, N.A. Technologies for municipal solid waste management: Current status, challenges, and future perspectives. *Chemosphere* **2022**, *288 Pt 1*, 132403. [CrossRef] [PubMed]
2. Vyas, S.; Prajapati, P.; Shah, A.V.; Varjani, S. Municipal solid waste management: Dynamics, risk assessment, ecological influence, advancements, constraints and perspectives. *Sci. Total Environ.* **2022**, *814*, 152802. [CrossRef] [PubMed]
3. Andeobu, L.; Wibowo, S.; Grandhi, S. Medical Waste from COVID-19 Pandemic—A Systematic Review of Management and Environmental Impacts in Australia. *Int. J. Environ. Res. Public Health* **2022**, *19*, 1381. [CrossRef] [PubMed]
4. Fazzo, L.; Minichilli, F.; Santoro, M.; Ceccarini, A.; Della Seta, M.; Bianchi, F.; Comba, P.; Martuzzi, M. Hazardous waste and health impact: A systematic review of the scientific literature. *Environ. Health* **2017**, *16*, 107. [CrossRef]
5. Montiel-Bohorquez, N.D.; Saldarriaga-Loaiza, J.D.; Perez, J.F. Analysis of investment incentives for power generation based on an integrated plasma gasification combined cycle power plant using municipal solid waste. *Case Stud. Therm. Eng.* **2022**, *30*, 101748. [CrossRef]
6. Kollu, V.K.R.; Kumar, P.; Gautam, K. Comparison of microwave and autoclave treatment for biomedical waste disinfection. *Syst. Microbiol. Biomanuf.* **2022**, *2*, 732–742. [CrossRef]
7. Tavares, R.; Ramos, A.; Rouboa, A. A theoretical study on municipal solid waste plasma gasification. *Waste Manag.* **2019**, *90*, 37–45. [CrossRef]
8. Li, H.; Sun, C.; Zhang, Y.; Li, T.; Wei, X. Performance investigation of the gasification for the kitchen waste powder in a direct current plasma reactor. *J. Energy Inst.* **2022**, *100*, 170–176. [CrossRef]
9. Ma, W.; Fang, Y.; Chen, D.; Chen, G.; Xu, Y.; Sheng, H.; Zhou, Z. Volatilization and leaching behaviour of heavy metals in MSW incineration fly ash in a DC arc plasma furnace. *Fuel* **2017**, *210*, 145–153. [CrossRef]
10. Zhang, K.; Harvey, A.P. CO₂ decomposition to CO in the presence of up to 50% O₂ using a nonthermal plasma at atmospheric temperature and pressure. *Chem. Eng. J.* **2021**, *405*, 126625. [CrossRef]
11. Dobslaw, C.; Glocker, B. Plasma Technology and Its Relevance in Waste Air and Waste Gas Treatment. *Sustainability* **2020**, *12*, 8981. [CrossRef]
12. Recebli, Z.; Selimli, S.; Ozkaymak, M.; Gonc, O. Biogas production from animal manure. *J. Eng. Sci. Technol.* **2015**, *10*, 722–729.
13. Sikarwar, V.S.; Hrabovská, M.; Oost, G.V.; Pohorelý, M.; Jeremiáš, M. Progress in waste utilization via thermal plasma. *Prog. Energy Combust. Sci.* **2020**, *81*, 100873. [CrossRef]
14. Gabbar, H.A.; Darda, S.A.; Damideh, V.; Hassen, I.; Aboughaly, M.; Lisi, D. Comparative study of atmospheric pressure DC, RF, and microwave thermal plasma torches for waste to energy applications. *Sustain. Energy Technol. Assess.* **2021**, *47*, 101447. [CrossRef]
15. Heberlein, J.; Murphy, A. B Thermal plasma waste treatment. *J. Phys. D Appl. Phys.* **2008**, *41*, 053001. [CrossRef]
16. Valdivia-Barrientos, R.; Ibañez-Olvera, M.; Pacheco-Sotelo, J.; Pacheco-Pacheco, M.; Estrada-Martinez, N.; Silva-Rosas, J.; Rivera-Rodríguez, C. Acid gas degradation by non-thermal plasma and energy estimation. *J. Phys. Conf. Ser.* **2012**, *370*, 012037. [CrossRef]
17. Prado, E.S.P.; Miranda, F.S.; de Araujo, L.G.; Petraconi, G.; Baldan, M.R. Thermal plasma technology for radioactive waste treatment: A review. *J. Radioanal. Nucl. Chem.* **2020**, *325*, 331–342. [CrossRef]
18. Leal-Quiros, E. Plasma Processing of Municipal Solid Waste. *Braz. J. Phys.* **2004**, *34*, 1587–1593. [CrossRef]
19. Sakhrjia, M.; Ramos, A.; Monteiro, E.; Bouziane, K.; Rouboa, A. Plasma gasification process using computational fluid dynamics modelling. *Energy Rep.* **2022**, *8*, 1541–1549. [CrossRef]
20. Li, Y.; Huang, Z.; Xu, Y.; Sheng, H. Plasma-arc technology for the thermal treatment of chemical wastes. *Environ. Eng. Sci.* **2009**, *26*, 731–737. [CrossRef]
21. Tang, L.; Huang, H.; Zhao, Z.; Wu, C.Z.; Chen, Y. Pyrolysis of polypropylene in a nitrogen plasma reactor. *Ind. Eng. Chem. Res.* **2003**, *42*, 1145–1150. [CrossRef]
22. Mountouris, A.; Voutsas, E.; Tassios, D. Solid waste plasma gasification: Equilibrium model development and exergy analysis. *Energy Convers. Manag.* **2006**, *47*, 1723–1737. [CrossRef]
23. Zhang, Q.; Dor, L.; Fenigshtein, D.; Yang, W.; Blasiak, W. Gasification of municipal solid waste in the plasma gasification melting process. *Appl. Energy* **2012**, *90*, 106–112. [CrossRef]
24. Favas, J.; Monteiro, E.; Rouboa, A. Hydrogen production using plasma gasification with steam injection. *Int. J. Hydrogen Energy* **2017**, *42*, 10997–11005. [CrossRef]
25. Janajreh, I.; Raza, S.S.; Valmundsson, A.S. Plasma gasification process: Modelling, simulation, and comparison with conventional air gasification. *Energy Convers. Manag.* **2013**, *65*, 801–809. [CrossRef]
26. COMSOL Multiphysics® V. 5.1. *CFD Module User's Guide*; COMSOL AB: Stockholm, Sweden, 2015; Available online: <http://www.comsol.com> (accessed on 1 November 2021).

27. Kuo, Y.M.; Chang, J.E.; Chang, Y.; Chao, C.C.; Tuan, Y.J.; Chang-Chien, G.P. Stabilization of Residues Obtained from the Treatment of Laboratory Waste. Part 1-Treatment Path of Metals in a Plasma Melting System. *J. Air Waste Manag.* **2010**, *60*, 429–438. [[CrossRef](#)]
28. Barjasteh, A.; Dehghani, Z.; Lamichhane, P.; Kaushik, N.; Choi, E.H.; Kaushik, N.K. Recent Progress in Applications of Non-Thermal Plasma for Water Purification, Bio-Sterilization, and Decontamination. *Appl. Sci.* **2021**, *11*, 3372. [[CrossRef](#)]
29. Li, J.; Liu, K.; Yan, S.; Li, Y.; Han, D. Application of thermal plasma technology for the treatment of solid wastes in China: An overview. *Waste Manag.* **2016**, *58*, 260–269. [[CrossRef](#)]
30. Zhao, P.; Ni, G.; Jiang, Y.; Chen, L.; Chen, M.; Meng, Y. Destruction of inorganic municipal solid waste incinerator fly ash in a DC arc plasma furnace. *J. Hazard. Mater.* **2010**, *181*, 580–585. [[CrossRef](#)]
31. Zhang, Q.; Dor, L.; Zhang, L.; Yang, W.; Blasiak, W. Performance analysis of municipal solid waste gasification with steam in a Plasma Gasification Melting reactor. *Appl. Energy* **2012**, *98*, 219–229. [[CrossRef](#)]
32. Gomez, E.; Amutha Rani, D.; Cheesemanb, C.R.; Deeganc, D.; Wisec, M.; Boccaccini, A.R. Thermal plasma technology for the treatment of wastes: A critical review. *J. Hazard. Mater.* **2009**, *161*, 614–626. [[CrossRef](#)] [[PubMed](#)]
33. Zhang, Q.; Dor, L.; Biswas, A.K.; Yang, W.; Blasiak, W. Modelling of steam plasma gasification for municipal solid waste. *Fuel Process. Technol.* **2013**, *106*, 546–554. [[CrossRef](#)]
34. Chiné, B. A 2D Model of a Plasma Torch. In Proceedings of the 2016 Comsol Conference, Munich, Germany, 12–14 October 2016; Available online: https://www.comsol.ch/paper/download/357271/chine_paper.pdf (accessed on 7 September 2022).
35. Mashayak, S.Y. CFD Modeling of Plasma Thermal Reactor for Waste Treatment. Master's Thesis, Purdue University West Lafayette, West Lafayette, IN, USA, August 2009.
36. Ibrahimoglu, B.; Cucen, A.; Yilmazoglu, M.Z. Numerical Modelling of DC Arc Plasma Torch with MHD Module. In Proceedings of the 1st International Plasma Technologies Congress, Kayseri, Turkey, 28–30 April 2014.
37. Soni, V.; Naik, V. Gasification—A Process for Energy Recovery and Disposal of Municipal Solid Waste. *Am. J. Mod. Energy* **2016**, *2*, 38–42. [[CrossRef](#)]
38. Bauchire, J.M.; Gonzalez, J.J.; Gleizes, A. Modeling of a DC Plasma Torch in Laminar and Turbulent Flow. *Plasma Chem. Plasma Process.* **1997**, *17*, 409–432. [[CrossRef](#)]
39. Anggraini, R.A.N.; Kusumandari, K.; Saraswati, T.E. Plasma reactor with continuous flow system for degradation of methylene blue. *AIP Conf. Proc.* **2018**, *2014*, 020037. [[CrossRef](#)]
40. Trelles, J.P.; Chazelas, C.; Vardelle, A.; Heberlein, J.V.R. Arc Plasma Torch Modeling. *J. Therm. Spray Technol.* **2009**, *18*, 5–6. [[CrossRef](#)]
41. Trelles, J.P.; Heberlein, J.V.R. Simulation Results of Arc Behaviour in Different Plasma Spray Torches. *J. Therm. Spray Technol.* **2006**, *15*, 563–569. [[CrossRef](#)]
42. Boulos, M.I.; Fauchais, P.; Pfender, E. *Thermal Plasmas: Fundamentals and Applications*, 1st ed.; Plenum Press: New York, NY, USA, 1994; 467p, ISBN 978-1489913388.
43. Li, H.P.; Zhang, X.N.; Xia, W.D. A numerical model of non-equilibrium thermal plasmas. II. Governing equations. *Phys. Plasmas* **2013**, *20*, 033509. [[CrossRef](#)]
44. Dedulle, J.M. Pedagogic using of COMSOL Multiphysics for learning Numerical Method and Numerical Modelling. In Proceedings of the Conference COMSOL Multiphysics, Paris, France, 12 December 2007.
45. Samal, S.; Blanco, I. An Overview of Thermal Plasma Arc Systems for Treatment of Various Wastes in Recovery of Metals. *Materials* **2022**, *15*, 683. [[CrossRef](#)]
46. Pfender, E.; Fincke, J.; Spores, R. Entrainment of Cold Gas into Thermal Plasma Jets. *Plasma Chem. Plasma Process.* **1991**, *11*, 529. [[CrossRef](#)]
47. Kuzenov, V.V.; Ryzhkov, S.V. The Qualitative and Quantitative Study of Radiation Sources with a Model Configuration of the Electrode System. *Symmetry* **2021**, *13*, 927. [[CrossRef](#)]
48. Bogaerts, A.; Tu, X.; Whitehead, J.C.; Centi, G.; Lefferts, L.; Guaitella, O.; Azzolina-Jury, F.; Kim, H.H.; Murphy, A.B.; Schneider, W.F.; et al. The 2020 plasma catalysis roadmap. *J. Phys. D Appl. Phys.* **2020**, *53*, 443001. [[CrossRef](#)]
49. Minutillo, M.; Perna, A.; Di Bona, D. Modelling and performance analysis of an integrated plasma gasification combined cycle (IPGCC) power plant. *Energy Convers. Manag.* **2009**, *50*, 2837–2842. [[CrossRef](#)]
50. Selvan, B.; Ramachandran, K.; Pillai, B.C.; Subhakar, D. Modelling of the plasma-substrate interaction and prediction of substrate temperature during the plasma heating. *Eur. Phys. J. D* **2011**, *61*, 663–675. [[CrossRef](#)]
51. Chen, X.; Geng, Y.; Fujita, T. An overview of municipal solid waste management in China. *Waste Manag.* **2010**, *30*, 716–724. [[CrossRef](#)] [[PubMed](#)]
52. Murashov, I.; Frolov, V.; Korotkik, M.; Ushomirskaya, L. Numerical simulation of DC air plasma torch modes and plasma jet instability for thermal spraying technology. *MATEC Web Conf.* **2018**, *245*, 04003. [[CrossRef](#)]
53. Duan, Z.; Heberlein, J. Arc Instabilities in a Plasma Spray Torch. *J. Therm. Spray Technol.* **2002**, *11*, 44–51. [[CrossRef](#)]
54. Trelles, J.P. Computational study of flow dynamics from a dc arc plasma jet. *J. Phys. D Appl. Phys.* **2013**, *46*, 255201. [[CrossRef](#)]
55. Cedzvnaska, K.; Kolacinski, Z.; Izydorczyk, M.; Sroczynski, W. Plasma vitrification of waste incinerator ashes. In *International Ash Utilization Symposium*; Center of Applied Energy Research, University of Kentucky: Kentucky, UK, 1999.
56. Bolot, R.; Li, J.; Coddet, C. Modeling of thermal plasma jets: A comparison between PHOENICS and FLUENT. In *ITSC2004*; ASM International: Almere, The Netherlands, 2004. [[CrossRef](#)]

57. Shumeiko, A.I.; Telekh, V.D.; Ryzhkov, S.V. Probe Diagnostics and Optical Emission Spectroscopy of Wave Plasma Source Exhaust. *Symmetry* **2022**, *14*, 1983. [[CrossRef](#)]
58. Lebouvier, A.; Delalondre, C.; Fresnet, F.; Boch, V.; Rohani, V.; Cauneau, F.; Fulcheri, L. Three-Dimensional Unsteady MHD Modeling of a Low Current—High Voltage Non-Transferred DC Plasma Torch Operating with Air. *IEEE Trans. Plasma Sci.* **2011**, *39*, 1889–1899. [[CrossRef](#)]
59. Li, H.; Li, T.; Wei, X. Main performance analysis of kitchen waste gasification in a small-power horizontal plasma jet reactor. *J. Energy Inst.* **2020**, *93*, 367–376. [[CrossRef](#)]
60. Franci lle, R.; Paulino, S.; Essiptchouk, A.M.; Costa, L.P.C.; Silveira, J.L. Thermodynamic analysis of biomedical waste plasma gasification. *Energy* **2021**, *244 Pt A*, 122600. [[CrossRef](#)]
61. Valmundsson, A.S.; Janajreh, I. Plasma gasification process modelling and energy recovery from solid waste. In Proceedings of the ASME 2011 5th International Conference on Energy Sustainability ES2011, Washington, DC, USA, 7–10 August 2011. [[CrossRef](#)]
62. Zhovtyansky, V.; Valin cius, V. Efficiency of Plasma Gasification Technologies for Hazardous Waste Treatment. In *Gasification for Low-Grade Feedstock*; Yun, Y., Ed.; IntechOpen: Rijeka, Croatia, 2018; Chapter 9. [[CrossRef](#)]
63. Selvan, B.; Ramachandran, K. Comparisons Between Two Different Three-Dimensional Arc Plasma Torch Simulations. *J. Therm. Spray Technol.* **2009**, *18*, 846. [[CrossRef](#)]
64. Achinas, S.; Kapetanios, E. Efficiency Evaluation of RDF Plasma Gasification Process. *Energy Environ. Res.* **2013**, *3*, 150–157. [[CrossRef](#)]

Disclaimer/Publisher’s Note: The statements, opinions and data contained in all publications are solely those of the individual author(s) and contributor(s) and not of MDPI and/or the editor(s). MDPI and/or the editor(s) disclaim responsibility for any injury to people or property resulting from any ideas, methods, instructions or products referred to in the content.